ELSEVIER

Journal of Nuclear Materials 307–311 (2002) 1643–1648

journal of nuclear materials

www.elsevier.com/locate/jnucmat

Some recent innovations in small specimen testing

G.R. Odette *, M. He, D. Gragg, D. Klingensmith, G.E. Lucas

Department of Mechanical and Environmental Engineering, University of California, Santa Barbara, CA 93106-5070, USA

Abstract

New innovative small specimen test techniques are described. Finite element simulations show that combinations of cone indentation pile-up geometry and load–penetration depth relations can be used to determine both the yield stress and strain-hardening behavior of a material. Techniques for pre-cracking and testing sub-miniaturized fracture toughness bend bars, with dimensions of $1.65 \times 1.65 \times 9$ mm^3, or less, are described. The corresponding toughness–temperature curves have a very steep transition slope, primarily due to rapid loss of constraint, which has advantages in some experiments to characterize the effects of specified irradiation variables. As one example of using composite specimens, an approach to evaluating helium effects is proposed, involving diffusion bonding small wires of a ^{54}Fe-based ferritic–martensitic alloy to a surrounding fracture specimen composed of an elemental Fe-based alloy. Finally, we briefly outline some potential approaches to multipurpose specimens and test automation.

1. Introduction

Small specimen test techniques have been an integral part of the development of materials for fusion reactor structures [1–3], largely as a result of limited irradiation volumes in various irradiation facilities such as fission test reactors and accelerator based high-energy neutron sources. We describe several new and innovative approaches to meeting the challenge of extracting mechanical properties and other information from very limited volumes of materials.

2. True stress–strain evaluations from indentation tests

A number of methods have been proposed for extracting true stress–strain constitutive relations, $\sigma(\varepsilon)$, from indentation tests. These techniques generally rely on either indentation load (P)–indentation depth (Δ_h) data (P–Δ_h) or characterization of the indentation pile-up height, h_p to width, L_{00}, aspect ratio, h_p/L_{00} [4–12]. We have previously shown that proposed empirical relations between instrumented ball indentation parameters and $\sigma(\varepsilon)$ are limited to a strain-hardening range ($N \approx 0.1$–0.2) and may be highly inaccurate at very low ε and for estimating yield stress, σ_y [13]. Moreover, we have also shown that h_p/L_{00}, are sensitive to the *average* strain-hardening behavior as, for example, represented by a power law exponent, N, over a relatively wide range of ε. However, h_p/L_{00} is relatively *insensitive* to the details of $\sigma(\varepsilon)$, particularly at very low (e.g., as needed for measuring σ_y) and high ε [14].

Based on finite element (FE) indentation simulations, we have recently developed a new method for more accurately determining σ_y using a combination of P–Δ_h and h_p/L_{00} measurements using a 68.2° rigid cone indentor. The simulations used the general purpose FE code ABAQUS [15]. The plasticity model in ABAQUS is based on J_2-incremental flow theory. Thus non-proportional and non-monotonic loading are well treated within the standard continuum assumptions of isotropic hardening and normality. The input to ABAQUS are the elastic modulus (E), the friction coefficient (μ), σ_y and the post-yield flow stress [$\sigma(\varepsilon)$] as a function of effective plastic strain (ε). The cone indentor was treated as two-dimensional (z, r, symmetric in θ) rigid body with

* Corresponding author. Tel.: +1-805 893 3525; fax: +1-805 893 8651.

E-mail address: odette@engineering.ucsb.edu (G.R. Odette).

0022-3115/02/$ - see front matter
PII: S0022-3115(02)01173-X

a variable friction coefficient. The mesh to model the two-dimensional half space has 1960 four-node quadrilateral axisymmetric elements and 2080 nodes. The radial (R) and depth (z) dimensions of the mesh were about $50\Delta_{max}$ and $20\Delta_{max}$, respectively, where Δ_{max} is the maximum penetration depth of the cone. Simulations were run for materials with constitutive behavior of the form

$$\varepsilon_p = \varepsilon_y(\sigma/\sigma_y)^{1/N}, \quad (1)$$

where $\varepsilon_y = \sigma_y/E$, with N varying from 0 to 0.3 and σ_y varying from 200 to 700 MPa.

Fig. 1(a) shows, that h_p/L_{00} decreases with increasing N, but is only slightly sensitive to σ_y, consistent with previous experimental observations [9,11]. In addition, h_p/L_{00} was found to be sensitive to μ only below $\approx$0.2, which was selected as the nominal baseline value. The corresponding P–Δ_h relation can be fit with a quadratic function,

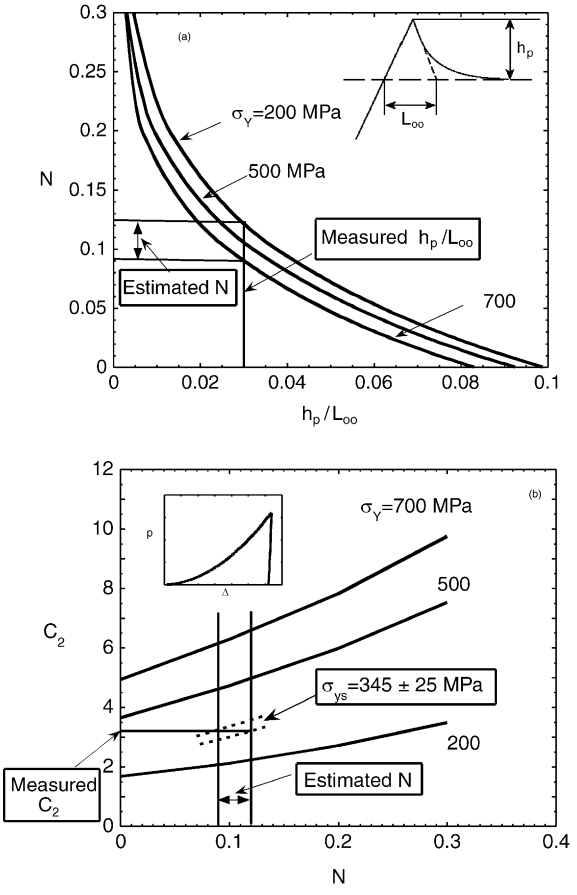

Fig. 1. Illustration of the procedure for first iteration to estimate N and σ_y: (a) variation of n with h_p/L_{00} and σ_y; (b) variation of C_2 with N and σ_y.

$$P = C_1\Delta_h + C_2\Delta_h^2. \quad (2)$$

Both C_1 and $C_2 = (d^2P/d\Delta_h^2)/2$ increase with N and σ_y. The variation, which is strongest with C_2, is shown in Fig. 1(b). This provides an opportunity to combine h_p/L_{00} and P–Δ_h data to estimate σ_y. Measured h_p/L_{00} is used first to estimate of N with some range of uncertainty ($N \pm \Delta N$) corresponding to an initial guess on the potential range of σ_y. The corresponding measurement of C_2 from the P–Δ_h curve is used in combination with $N \pm \Delta N$ to estimate a range of $\sigma_y \pm \Delta\sigma_y$. This is repeated iteratively, thus narrowing the range of both σ_y and N. Note this procedure is not restricted to $\sigma(\varepsilon)$ in the form of Eq. (1). The N derived for materials with more complex relations, such as alloys with Luder's type strain regions, represents an average strain-hardening behavior over a range of ε from $\approx$0.01 to $\approx$0.25. Future work will extend the investigation to other indenter shapes, and experimental testing is planned.

3. Microminiaturized fracture specimen tests

A microminiaturized fracture test has been developed to increase the number of specimens accommodated in a limited irradiation volume. These tests, which also minimize the radioactivity and may permit out-of-cell testing, can be used to *estimate* the position of a master curve (MC) of the toughness–temperature $K_{Jc}(T)$ relation and to evaluate irradiation induced temperature shifts in large matrix single-variable experiments. They will also be used to enable high-energy proton irradiation studies.

The microminiaturized three point bend bar fracture specimen represents a pre-cracked version of a specimen that is also used for a variety of deformation studies, including beam bending, notched beam bending and hardness transverses on the sides of bent beams sections to asses flow stress at high strains. The so-called deformation and fracture mini-beam (DFMB) has a baseline thickness (B), width (W) and length (L) dimensions of $B = 1.65 \times W = 1.65 \times L = 9$ mm, equivalent to a $\approx$1/6 Charpy specimen. In the case of fracture testing, the DFMB is pre-cracked to a length (a) to W ratio a/W, typically about 0.35–0.45. A total of 216 DFMB specimens can be accommodated in a single Charpy volume. However, all DFMB dimensions and a/W can be adjusted to any selected configuration.

Convenient preparation of these fracture DFMB specimens is enabled by a special pre-cracking procedure. First, a large bend bar parent is carefully pre-cracked to an $a/W \approx 0.5$. The W can vary with the availability of material but is typically $\geqslant$5–10 mm. However, the corresponding B can be even larger, with typical values in the range of 25–50 mm. The pre-cracked parent is then sectioned into a large number of

much thinner bars with the DFMB thickness (B), but still with the original parent W. The pre-crack tips are then located in each of the thinner sections and the fronts and backs of the bars machined off in a special fixture to produce the final pre-selected W and a/W.

The pre-cracked DFMB specimens are tested on an instrumented drop tower, using a large mass and a low drop height of 3–6 mm to reduce the measured impact velocity and minimize inertial oscillations. Impact tests are preferred compared to static tests since they elevate the transition temperature regime, facilitating testing and analysis of the data. The tests are conducted in a temperature-controlled chamber from about -190 to $+200$ °C measured by several calibrated thermocouple monitors. Dynamic toughness as a function of test temperature, $K_{md}(T)$, is determined from impact load–time–displacement (P–t–d) curves obtained from a calibrated instrumented TUP. Typical stress intensity rates are on the order of several thousand MPa$\sqrt{}$m/s. The subscript md for the K_{md} refers to an effective dynamic toughness obtained from the microminiaturized specimens. Use of a reference K_{md} in the range of 50–70 MPa$\sqrt{}$m reduces the temperature shifts due to constraint loss [17] and can be used to define a corresponding reference T_{md} based on a limited number of tests of the DFMB specimens. Statistical considerations suggest that a minimum of 12 tests in the transition (at a mean $K_{md} \approx 60$–80 MPa$\sqrt{}$m) are desirable and yields a T_{md} with a relatively small margin of uncertainty of less than $\approx \pm 10$–15 °C.

Fig. 2 shows a $K_{md}(T)$ data for an A533B pressure steel taken from the vessel of the decommissioned Shoreham nuclear power plant and the IEA heat of the F82H martensitic steel. A typical sharp pre-crack emanating from the starter notch is also shown. As can be seen $K_{md}(T)$ exhibits a very sharp transition relative to large specimen data, as characterized by the estimated position of a dynamic MC for these steels shown by the dashed lines. As discussed elsewhere, the sharp transition is due to both loss of constraint and, possibly, statistical effects in the very small DFMB [17]. Constraint and statistical effects also results in a large decrease in the static DMFB transition region relative to the T_0 found for static MC tests on larger specimens [16,17]. However, this downward shift in is partially to fully compensated by an upward temperature shift at the dynamic versus static loading rate. Thus T_{md} is expected to occur in the 'vicinity' of the MC T_0.

Fig. 3 shows the P–t curves and fractographs associated with the changes in the fracture processes with increasing temperature for the F82H steel. At low temperature and K_{md} failure is entirely by linear elastic cleavage. In the knee and lower transition toughness region, the fracture is elastic–plastic following general yielding. In this case unstable cleavage initiation is terminated by crack arrest followed by ductile tearing to complete specimen separation. At still higher temperatures, on the upper shelf, crack growth initiation is by microvoid coalescence and ductile tearing. The corresponding P–t curves reflect this test temperature dependent sequence of failure processes in a way that is completely analogous to standard fracture tests. Thus even with their very small dimensions, the DFMB provide *real fracture data*, pertinent to both assessment of material performance and use in single variable experiments.

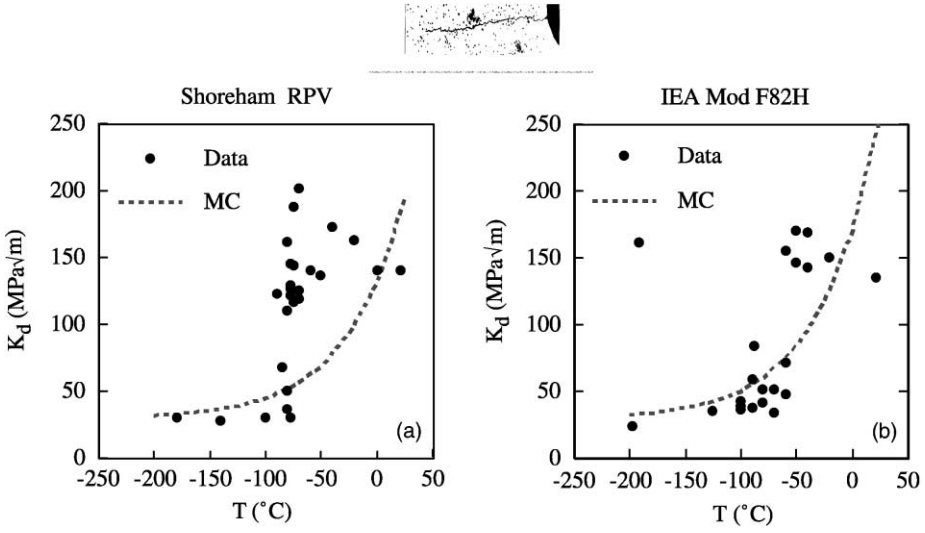

Fig. 2. Variation of toughness with temperature for tests on DFMB specimens of (a) Shoreham A533RPV plate and (b) IEA F82H. The estimated MC adjusted for the dynamic loading rate is shown for comparison. A typical pre-crack emanating from a starter notch is also shown.

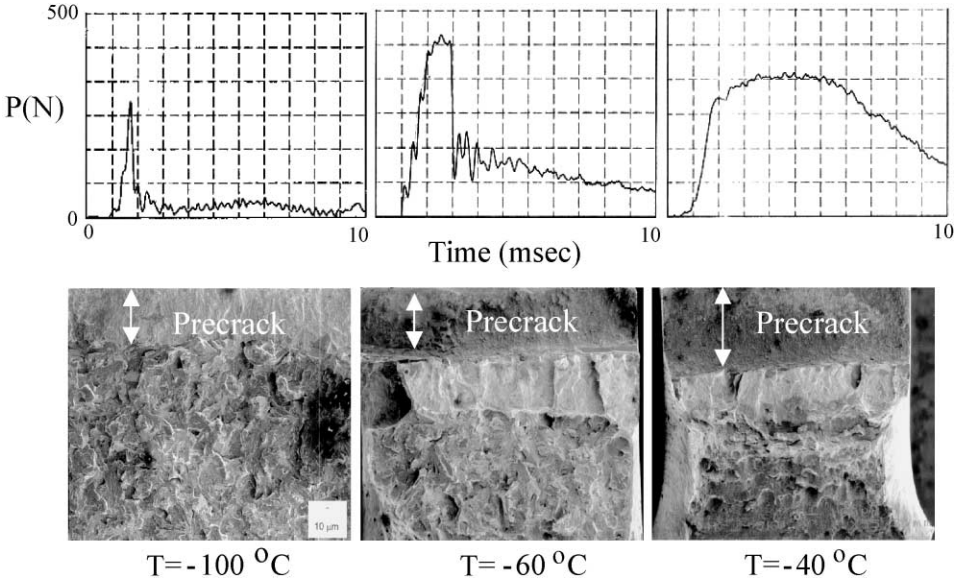

Fig. 3. Load–time (P–t) and fractographs for a sequence of DFMB tests on F82H at increasing temperature.

However, the pre-cracked DFMB-T_{md} test is not really intended to replace more direct measurements of the T_0 for MC fracture toughness $K_{Jc}(T)$. Nevertheless the very sharp transition and good statistics make these specimens very attractive for assessing effects of specific variables on transition temperature shifts in irradiation experiments. For example, plans are being developed to use these DFMB specimens in experiments to distinguish possible effects of He on fast fracture from classical embrittlement due to irradiation hardening.

4. Composite fracture specimen

A number of approaches to application of composite fracture specimens have proven successful, such as the reconstitution of broken Charpy into PCC fracture specimens [18]. The general principle is to join a smaller volume of material of direct interest to generally larger volumes of material that provide for requisite load transfers and, in some cases, limitations on the amount of plastic deformation that lead to loss of constraint. In most past instances composite specimens are fabricated by fusion welding after conditioning treatments such as irradiation. However, in cases where the amount of material of interest presents the primary limitation, *prefabrication* of composite specimens *before conditioning* presents a great and largely unexploited opportunity.

One (of many) example of an approach to using composite specimens is our proposal to use a very limited amount of ^{54}Fe to evaluate the effects of He on fast fracture. Relatively high levels of He and H are produced by two step thermal neutron reactions, with the first leading to the formation of the ^{55}Fe with high thermal neutron n,α and n,p cross-sections. Irradiation in mixed spectrum reactor environments, with high thermal to fast flux ratios, lead to the production of He in ^{54}Fe at a rate of about 2–4 appm/dpa (and even larger amounts of H) [19]. Thus, high fluence irradiation can produce high quantities of He. This concept has been exploited in the so-called FIST experiments that have used F82H type steel alloys enriched in ^{54}Fe to measure changes in strength, helium and hydrogen levels and microstructure in 3×0.2 mm sized TEM discs [19]. However, a major limitation in the ^{54}Fe tailoring approach is the high cost of separated ^{54}Fe which is on the order of \$20 000/g. Thus fabrication of fracture specimens has been considered to be prohibitively expensive.

We have proposed a way to produce a large number of pre-fabricated composite fracture specimens with a very limited amount of ^{54}Fe. In this case the ^{54}Fe based alloy would be limited to the fracture process zone around the crack, and hence, need only compose a small fraction of the overall volume of a specimen. The process zone for cleavage is on the order of 2–10 times the critical crack mouth opening displacement, $\delta = 0.5K_I^2/E\sigma_y$ where E is the elastic modulus. Thus for a typical combinations of $K_{Jc} = 100$ MPa$\sqrt{\text{m}}$, $\sigma_y = 700$ MPa and $E = 200$ GPa, the maximum process zone size is less than about 350 μm. Note that this is significantly smaller than the corresponding plastic zone size on the order of 1000 μm.

The fabrication of the composite specimens involves embedding small sections of ^{54}Fe alloy in a large matrix of an ordinary alloy of interest by diffusion bonding. The composite is then heat treated to produce a uniform

elemental composition and microstructure. Typical ferritic–martensitic steels would be austenitized, quenched and tempered. A significant challenge is to produce very small heats of ^{54}Fe isotopically tailored alloys with appropriate microstructures and compositions. However, we believe this can be achieved with an appropriate development effort. After heat treatment, the actual specimens would be machined and pre-cracked, with the crack tip located just inside the ^{54}Fe enriched process zone region.

A number of different configurations for the ^{54}Fe composite specimen can be envisioned, and the specifics can be tailored to a particular need. As an example, very fine ^{54}Fe alloy wires with a diameter of 500 μm could be fabricated and bonded to fairly large compact tension or bend bar specimens, say with a nominal thickness of 3.3 mm. Not considering the effect of alloy elements or machining, only 1 cm^3 of ^{54}Fe (7.9 g) would be sufficient to produce about 1500 fracture specimens. We plan to include composite ^{54}Fe specimens in future US-JAERI irradiation experiments in the HFIR reactor.

Another example of potential pre-fabricated composite specimens is the use of in situ implantation from regions of high He generation rate (e.g., containing Ni or B in mixed spectrum reactors) into regions of interest. For example, implantation near grain boundaries in martensitic steels or vanadium alloys could be used to study helium bubble formation and growth under irradiation and stress. Finally, we note that the relatively simple and well-developed Charpy-type method of reconstitution of fracture specimens after irradiation of smaller pre-cracked sections presents a significant space saving opportunity.

5. Multipurpose specimens, pre-configured specimens and automated testing

Previous experience has shown the benefits of using a single specimen for multiple post-irradiation characterization studies. For example, 1 mm discs have been used for TEM studies after they had been produced in a shear punch test on 3 mm discs [19]. We have commonly used stacks of 1/3-sized Charpy bars in small angle neutron scattering (SANS) studies; and microhardness can be used in almost any specimen configuration without compromising its intended purpose. However, this experience has most often involved an after-the-fact insight, rather than a planned series of tests. Thus, there is a great opportunity to optimize of multipurpose a specimen testing by using specimen configurations coupled to a series of pre-planned, non-destructive or quasi-non destructive characterization techniques. For example, small general purpose coupons, including those in the form of tensile specimens, can be used for microhardness, SANS, resistivity, Seebeck coefficient, positron annihilation, shear punch and beam bending measurements, with the remnants available for TEM and atom probe studies. While space does not permit detailed descriptions, in many cases the testing methods can partially or fully automated, as we have done for both tensile and microhardness measurements. Finally, we note the advantage of pre-configuring specimens for their intended purpose can, in some cases, greatly facilitate testing. For example irradiation of thin foils for X-ray scattering studies and small bars for atom probe and fracture surface spectroscopy studies are only two of a number of examples.

6. Summary and conclusions

A variety of new and innovative small specimen test techniques have been proposed in this paper. While they are at various stages of development, all share a common approach based on physical understanding of the underlying deformation and fracture processes and, where possible, application of quantitative models for both test design and data analysis. The benefits of the use of multiple purpose specimens, test automation and optimizing specimen configurations have also been emphasized.

However, a more important and fundamental point is the need to pose the *critical questions* that are to be answered in any irradiation experiment; and to use fully *integrated* experimental designs, including consideration of post-irradiation characterization and innovative specimens and tests, to provide *focussed answers*. It is also necessary to integrate experiments and modeling. This new paradigm is a considerable improvement over simple empiricism, and will greatly expand the set of tools available to the fusion materials community to gain both a fundamental understanding of flow and fracture behavior as well as develop improved materials to serve in the fusion environment.

Acknowledgement

This work was supported in part by the US Office of Fusion Energy Sciences, grant number DE-FG03-94ER54275.

References

[1] W.R. Corwin, G.E. Lucas (Eds.), The use of small-scale specimens for irradiated testing, ASTM-STP-888, American Society for Testing and Materials, Philadelphia, PA, 1986.
[2] G.E. Lucas, Metall. Trans. 21A (1990) 1105.
[3] P. Jung, A. Hishinuma, G.E. Lucas, H. Ullmaier, J. Nucl. Mater. 232 (1996) 186.

[4] P. Au, G.E. Lucas, J.W. Sheckherd, G.R. Odette, Flow property measurements from instrumented hardness tests, Non-destructive Evaluation in the Nuclear Industry, Metals Park, OH, 1980, p. 597.
[5] F.M. Haggag, G.E. Lucas, Metall. Trans. 14A (1983) 1607.
[6] K. Shinohara, G.E. Lucas, G.R. Odette, J. Nucl. Mater. 133&134 (1986) 326.
[7] G.E. Lucas, Metall. Trans. A 21A (1990) 1105.
[8] R. Boklen, in: J. Westbrook, H. Conrad (Eds.), The Science of Hardness Testing and Its Applications, ASM, Metals Park, OH, 1973, p. 109.
[9] K. Furuya, J. Moteff, Metall. Trans. A 12A (1981) 1303.
[10] M. Jayakumar, G.E. Lucas, J. Nucl. Mater. 122&123 (1984) 840.
[11] C. Santos, G.R. Odette, G.E. Lucas, T. Yamamoto, J. Nucl. Mater. 258 (1999) 452.
[12] F.M. Haggag, R.K. Nanstad, J.T. Huton, D.L. Thomas, R.L. Swain, Use of automated ball indentation testing to measure flow properties and estimate fracture toughness in metallic materials, in: A.A. Braun, N.E. Ashbaugh, F.M. Smith (Eds.), Applications of Automation Technology to Fatigue and Fracture Testing, ASTM 1092, American Society for Testing and Materials, Philadelphia, 1990, p. 188.
[13] Y.M. He, G.R. Odette, G.E. Lucas, Spherical indentation and flow property measurement-finite element simulation, MRS Symp. Proc. 649, in press.
[14] Y.M. He, G.R. Odette, G.E. Lucas, B. Schroeter, ASTM STP 1418, American Society for Testing and Materials, West Conshohocken, PA, in press.
[15] ABAQUS Users Manual 5.8, Hibbit, Karlsson and Sorenssen, 1998.
[16] G.R. Odette, K. Edsinger, G.E. Lucas, E. Donahue, in: W.R. Corwin, S.T. Rosinski, E. van Walle (Eds.), Small Specimen Test Techniques, ASTM-STP-1328, American Society for Testing and Material, Philadelphia, PA, 1998, p. 298.
[17] G.R. Odette, Y.M. He, Micromechanical modeling of MC temperature shifts due to constraint loss, these Proceedings.
[18] E. Klausnitzer, Werkstofftechnik 7 (10) (October 1897) S.257.
[19] D.S. Gelles, M.L. Hamilton, B.M. Oliver, L.R. Greenwood, Recent results for the ferritics isotopically tailoring (FIST) experiment, these Proceedings.